Surgical and Radiologic Anatomy (2019) 41:401–408
https://doi.org/10.1007/s00276-019-02190-2

ORIGINAL ARTICLE

The adaption of the bony microstructure of the human glenoid cavity as a result of long-term biomechanical loading

Sebastian Hoechel[1] · Tibor Andrea Zwimpfer[1] · Mireille Toranelli[1] · Magdalena Müller-Gerbl[1]

Received: 30 May 2018 / Accepted: 17 January 2019 / Published online: 1 February 2019

Abstract

Structural arrangements of the bony microstructure of a joint through adaptational processes are thought to be determined by the biomechanical demands and its changes. Pursuing this theory of "form follows the biomechanical function", the load distribution of the glenoid cavity, as it is mirrored in its mineralization pattern, should link not only to its thickness distribution, but also will have an impact onto the trabecular network below. To prove and confirm this hypothesis, we analysed the mineral distribution in correlation to the subchondral bone plates thickness and the distribution of architectural parameters of the trabecular network below. Our findings clearly state an inhomogeneous but regular and reproducible mineral distribution pattern in respect to the biomechanical demands and a thickness of the subchondral bone plate which shows a significant correlation (78–93%). As for the trabecular network below, the distribution of the analysed parameters also revealed an inhomogeneous distribution with a regular pattern in correlation to the biomechanical impact. We found distinctive maxima of material distribution and stability (bone volume 79%, plate-like architecture 77%) situated below areas of high long-term load intake. With increasing depth, the trabecular network administers the expression of each structural parameter following the fact that the strain energy gets more and more evenly distributed and changes from a high degree of differentiation just beneath the SBP to a more equal distribution within the deeper areas. After all, the biomechanical situation of a joint directly influences the bony formation of the subchondral bone plate and the trabecular network below.

Keywords Glenoid cavity · Subchondral bone plate · Long-term load intake · Trabecular architecture · Micro-computed tomography

Introduction

Since the assumption of the correctness of Wolff's law in material science, researchers accept the idea that mechanical loading ultimately alters and determines the macro- and micro-anatomy of the human skeleton [34]. Structural differences and adaptational processes are therefore determined by the physical lifestyle such as daily activities as well as biomechanical changes due to injuries to the musculoskeletal system.

In detail, we know that bone growth begins in utero and continues until adolescence. After the growth period where genetic predispositions are dominating, bones respond via cellular and molecular mechanisms to mechanical stress via modelling and remodelling. If bone strain exceeds a modelling threshold of about 1000 micro-strains in the younger adult, bone formation starts, long-term strains below that level stop the formation process or even lead to resorption [6]. Combining both processes, the skeletal system shows a continuous process of bone renewal and an adaptation to the present mechanical loading situation.

As shown in recent literature, small changes in strain may result in large changes in principal material orientation, since the cells of bone indeed respond to biomechanical forces [5]. More recently, the maintenance and adaptation of bone formation were studied by Huiskes et al. using the finite element method. The results do show that cell activity is governed by feedback from biomechanical load transfer of the subchondral bone plate (SBP) down

Sebastian Hoechel and Tibor Andrea Zwimpfer contributed equally to this work.

✉ Sebastian Hoechel
sebastian.hoechel@unibas.ch

[1] Department of Biomedicine, Musculoskeletal Research, University of Basel, Pestalozzistrasse 20, 4056 Basel, Switzerland

into the trabecular network (TN) [16]. The biomechanical characteristics of the developing system seem to have an optimal mechanical structure with highest stability by the least material used.

Altogether, the adaptation of bone within the SBP and TN are dependent on the long-term biomechanical loading defined by the static and dynamic pressure distribution.

Different studies have demonstrated that the SBP shows a functional adaption to its long-term biomechanical loading by distributing the mineral content as to best serve the demands and generates distribution pattern of its mineralization unique to each human and joint [9, 15, 19].

For the glenoid cavity (GC), the shallow, pyriform articular surface of the glenohumeral ball joint (human shoulder joint), a monocentric and bi-centric mineralisation pattern within the SBP are described. This is interpreted as a result of the biomechanical loading pattern which can be considered as an expression of functional shoulder activities [19, 21].

Since the impact force experienced by the joint is transmitted through the SBP into the TN, the subarticular cancellous bone also exhibits structure-dependent topographical differences. Analysing computer-tomographic (CT) scans, Frich et al. described the regional variations in trabecular bone architecture in terms of orientation and density distribution. In their study, they found the peak density and most perpendicular orientation to be along the anterior rim of the glenoid [12]. Although the results are remarkable accurate, the disadvantage of this method is the interpretation of two-dimensional sections for extrapolation of the three-dimensional (3D) arrangement which consistently leads to false assumptions [10].

Today, micro-computer tomography (micro-CT) presents an emerging alternative to the radiologic analysis of serial sections, since it was shown that deriving bone parameters of the TN using interpolations of two-dimensional sections leads to incorrect results which tend to be smaller in comparison to measurements obtained in 3D [1, 7].

For a better understanding of the biomechanical effects onto the GC, we investigated the theory of "form follows the biomechanical function" and link the load distribution of the glenoid cavity`s SBP to the architecture of the supporting TN. Therefore, we used the established method of computed tomography osteoabsorptiometry (CT-OAM) to describe the long-term biomechanical intake of the SBP via its density distribution and correlated the results in respect to the trabecular architecture acquired using 3D micro-CT datasets based on a modified Feldkamp algorithm [11, 23].

This way, we can illustrate the architectural arrangement of the TN in direct relation to the biomechanical long-term load intake and describe the mechanical adaptations of bone. Next to the biomechanical interest of the results, it furthermore is of significance for prosthesis design. Here, the question of best fixation and therefore placement of the subcortical screws could be supported [31, 32].

Material

Twelve formalin-fixed human GC samples (5 male, 6 female; 11 right, 1 left; age 60–74 years, mean 70.2 years; unknown medical history; Institute of Anatomy Basel—CH; and Ludwig Maximilian University of Munich—D) were analysed.

Prior to the analysis, all samples were dissected free of soft tissue to improve scan quality. The degeneration score was assessed in accordance to Kellgren and Lawrence (3 × grade 0; 4 × grade 1; 5 × grade 2; grade 3 and 4 were excluded) [18].

In consideration of "The Code of Ethics of the World Medical Association" (Declaration of Helsinki), for experiments involving humans, the samples were taken from body donors to the Departments, who contributed their body to science and research only.

Methods

Computed tomography osteoabsorptiometry

To evaluate the mineralisation pattern of the SBP by means of CT-OAM, we used a conventional CT scanner (SOMATOM Emotion 16 SL, Siemens, Erlangen, Germany, 120 kV, 180 mA s). The axial section thickness of 0.6 mm was consequently orientated according to regular patient position. The recorded CT datasets were evaluated using the image analysing software ANALYZE® 11.0 (Biomedical Imaging Resource, Mayo Foundation, Rochester, MN, USA). The acquired reconstructions of the GC were arranged in frontal view to the joint surface. Using a "maximum intensity projection" algorithm, the highest density values of the SBP were projected onto the surface and assigned to a predefined colour map. The most dense voxels (> 1200 HU) were typified black, followed by the shading colours of red, yellow, green and blue (steps of 200 HU in descending order) (Figs. 1, 2).

For the evaluation of the final density distribution pattern and the correlation to localized values of trabecular architecture, we divided the joint surface into squares, seven in cranio-caudal orientation and five in anterior–posterior orientation. Each square was defined as a region of interest (ROI) and consequently numbered. For each ROI, an average mineralization in direct proportion to its density distribution was assessed [14, 23–25].

The method of CT-OAM was validated using dual-energy quantitative CT with a discrepancy of 0.5% in comparison to the analysis of fresh and frozen samples [22]. Therefore,

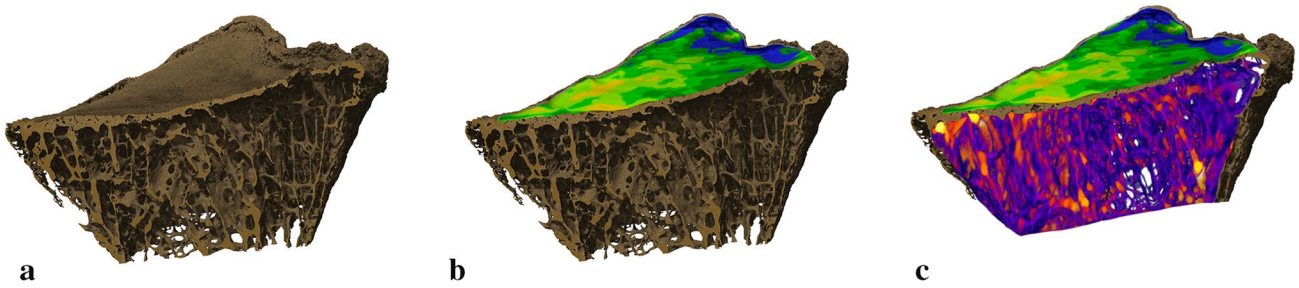

Fig. 1 Illustration of measurement methods. **a** 3D reconstruction of one glenoid cavity (same as Fig. 2a). **b** Colour-coded distribution of mineralization of the subchondral bone plate projected onto the 3D reconstruction. **c** Relative distribution of bone volume of the trabecular network below the subchondral bone plate

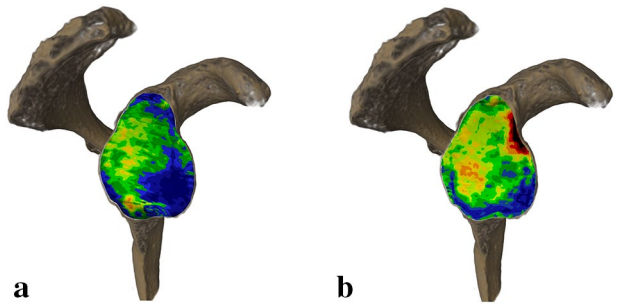

Fig. 2 Glenoid cavity (lateral view) with superimposed mineral distribution. **a** Monocentric distribution pattern. **b** Bi-centric distribution pattern

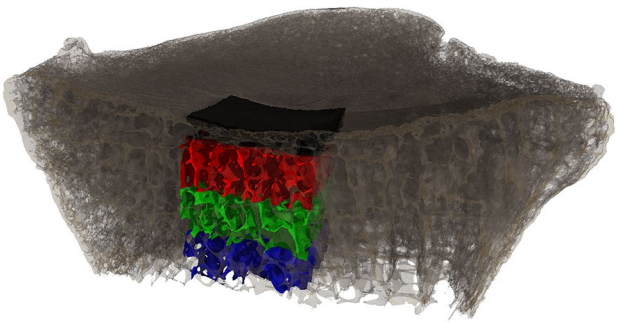

Fig. 3 Method of micro-CT analysis. Definition of volumes of interest (VOI) below the region of interest, ROI = black. (1st VOI 0–1 mm: red; 2nd VOI 1–2 mm: green; 3rd 428 VOI 2–3 mm: blue)

the density distribution with respect to the HU directly links to the calcium-hydroxyapatite concentration which was calculated and used for analysis here.

The trabecular structure analysed by micro-computed tomography

In a first step, we compiled 3D reconstructions of the CG using a General Electric phoenix nanotom® m system (Wunstorf, Germany) with an acceleration voltage of 140 kV, beam current of 60 µA, and a 0.1 mm aluminium filter to reduce beam hardening.

The scans were performed in sagittal direction with an equal voxel size of 20 µm for all samples. 3000 pictures each were acquired and a 3D reconstruction according to the Feldkamp algorithm was conducted [5].

Second, we prepared the data with the help of the analysing software VG-Studio® MAX 2.1 (Heidelberg, Germany) and adapted the volumes of interest (VOI) for trabecular analysis in agreement with the defined ROIs of the mineralization analysis. By definition, we assigned three VOIs into the depth below every single ROI. Each VOI covered a depth of 1 mm. This way, the trabecular structure was analysed into a depth of 3 millimetres below every ROI (Fig. 3).

After defining the ROIs and VOIs, we assessed the thickness of the SBP followed by the acquisition of the main parameters of trabecular bone architecture (for each VOI in a single matter) relevant to the current literature with the help of the analysing software CT-analyser® (Bruker-Micro-CT; Belgium) [13, 28].

Obtained parameters of trabecular architecture

The obtained parameters of bone histomorphometry and architecture were selected according to literature recommendations of bone analysis [8, 13].

Parameters of primary measurements in bone histomorphometry:

BV/TV (%), the fraction of bone volume in regards to the total volume;

BS/TV (1/mm), the bone surface present within the total volume;

Tb.Th (mm), the mean thickness of the trabeculae; and

Tb.Sp (mm), the trabecular spacing as parameter of the mean distance between each single trabecular.

Derived indices:

Tb.N (1/mm), trabecular number per volume as structural parameter.

As well as:

SMI (dimensionless), quantifies the characteristic form of a three-dimensionally described structure in terms of the amount of plate- and rod-composing parts of the structure. For an ideal plate and rod structure, the SMI value is 0–3, respectively; and

DA (dimensionless), the degree of anisotropy to directly quantify how highly oriented substructures are within a volume of trabecular bone.

For visualization of the results, all data was demonstrated in 2D distribution charts.

Statistical analysis

Distributional analysis was performed for every ROI, as for comparison, depth-based data analysis was performed for every VOI. The datasets were analysed regarding each sample individually.

Statistical analysis included the Pearson product-moment correlation coefficient and a two-tailed *t* test stating the significance. All analyses were performed using RStudio (RStudio: Integrated-development environment for R, Version 0.99.467, Boston, MA, USA).

Results

Mineralisation and thickness distribution of the SBP of the GC

The results show that the density distribution and therefore the mineralisation is inhomogeneous. Areas with high and lower mineral content can be detected which are distributed in a reproducible and organized manner revealing two different main distribution pattern. 5 samples could be attributed to a monocentric distribution pattern, 7 to a bi-centric model.

The peak mineralisation spot within the monocentric categorized samples was found consistently on the middle posterior area of the GC. The bi-centric distributed samples showed an additional area of high calcium-hydroxyapatite concentration situated in the middle parts of the anterior rim (Fig. 2). The peak values of the mineralisation showed inter-individual differences between 900 and 1000 mg/ml calcium-hydroxyapatite, while the low value range was found to be between 350 and 450 mg/ml.

Concerning the thickness of the SBP, we found a solid wave-like lamella with an overall volume of 94–96% (SD 3.4) of bone. The solid structure was only interrupted by identified nutrient canals running upwards into the cartilage of the joint surface. The thickness distribution was found to be correlating to the mineral distribution described above with a range of 78–93% (SD 4.3) and resembled statistical significance ($p < 0.01$). The maxima of SBP thickness was assessed to be up to 0.89 mm (SD 0.16), and the minimum thickness was around 0.46 mm (SD 0.14). The difference of maxima and minimum was statistically significant ($p < 0.01$).

Distribution of parameters of trabecular network architecture and the correlation to the mineral distribution of the SBP above

The trabecular architecture presented itself as inhomogeneous throughout the glenoid cavity with a certain regularity of distribution below the SBP across the articular surface as well as into depth.

BV/TV

The distribution of the bone volume was inhomogeneous within each analysed millimetre of depth. Maxima were found beneath areas of peak mineral concentration according to the centric classification. Within the VOIs of the first analysed mm, an overall distribution was found which had a calculated correlation to the described mineralisation of the SBP of 79%. The pattern of distribution of bone volume within the first millimetre showed a consistency into depth with a gradually decreasing range of the maximum–minimum values (Fig. 4). The correlation to the mineral distribution lessened to 46% within the third millimetre (Table 1).

BS/TV

As observed above, there was an inhomogeneous distribution with a stable distribution pattern. Maxima were located below the middle posterior facet. The bi-centric samples with an additional one were located beneath the middle/superior anterior rim. The absolute values here as well showed a diminution with every millimetre of depth (Fig. 4). The correlation to the mineral content of the SBP also lessened with depth (Table 1).

Tb.Th and Tb.N

The maxima of trabecular thickness and number were found to be in correlation to the bone volume below the middle of the posterior facet and the superior anterior rim. The absolute correlation decreased down to the third millimetre as the distribution got more even (Fig. 4; Table 1).

Tb.Sp

The distribution pattern of the spacing differed in regard to the above-described parameters. Contrary to the parameters describing bone being present, here we found a minimum below the middle of the posterior facet and anterior superior

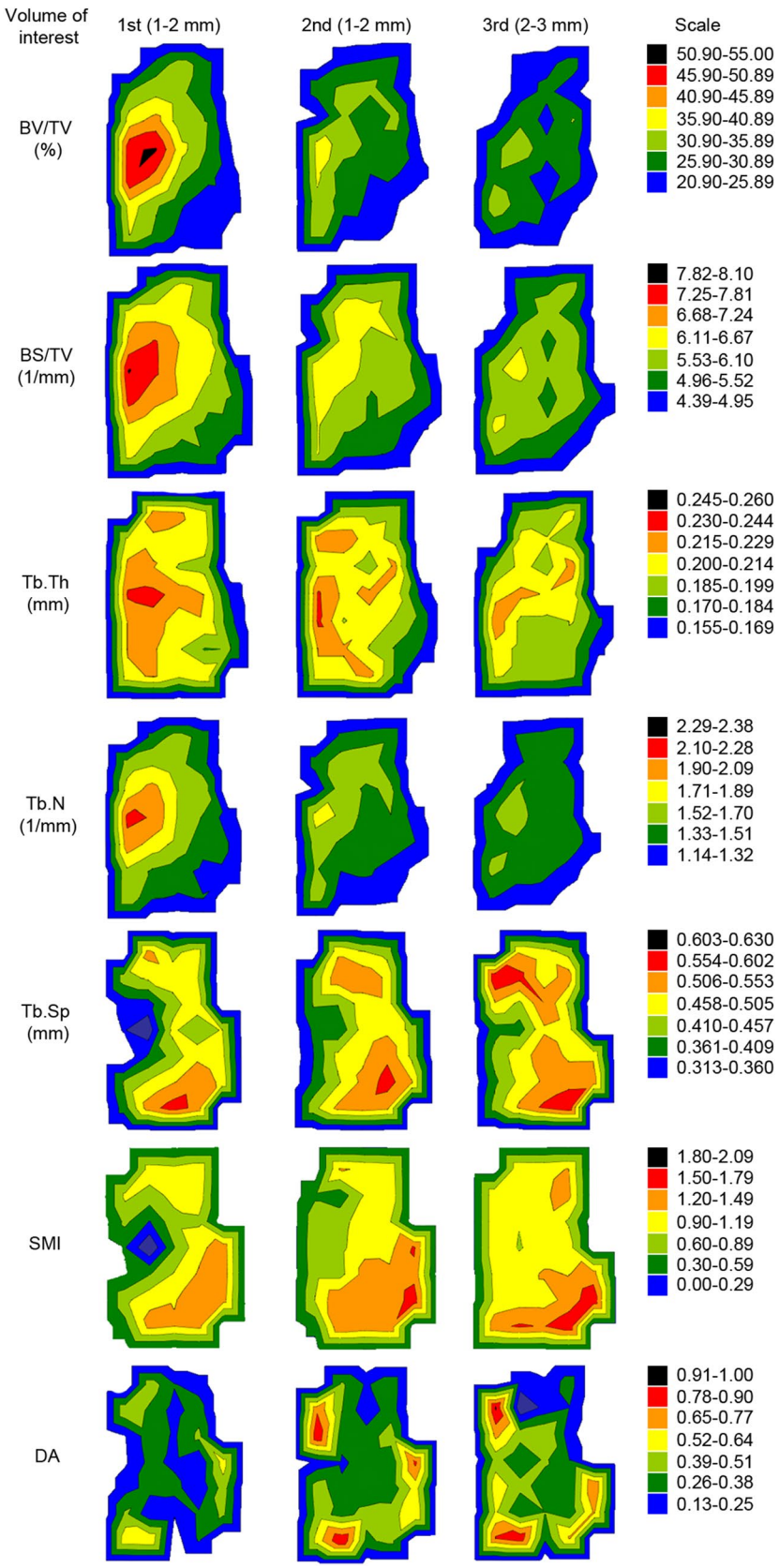

Fig. 4 2D distribution charts of trabecular architectural parameters for the three analysed VOIs from the first to the third millimetre (same monocentric sample as Figs. 1, 2a)

Table 1 Correlations of trabecular bone of: mineral distribution of the subchondral bone plate and the architectural parameters

	BV/TV	BS/TV	Tb.Th.	Tb.N.	Tb.Sp.	SMI	DA
0–1 mm	0.79	0.75	0.70	0.69	− 0.75	− 0.77	− 0.71
1–2 mm	0.61	0.58	0.50	0.54	− 0.39	− 0.56	− 0.65
2–3 mm	0.46	0.50	0.42	0.32	− 0.23	− 0.45	− 0.34

rim. The highest absolute values were present below the inferior parts of the articulation surface. Overall, the absolute numerical values showed an increasing behaviour into depth as the overall spacing increased (Fig. 4). Concerning the correlation coefficient to the mineralisation of the SBP, we found high negative values with the VOIs of the first millimetre which increased with depth (Table 1).

SMI

Within the analysed sample population, we found plate-like trabecular mainly below areas of peak mineral content within the SBP. Rod-like architectural components were seen below parts with less mineralization above, while a plate-like state was present below wares of high mineralization and biomechanical demands. This distribution pattern continued down to the third millimetre, while the absolute values of the SMI increased, accounting for an overall more rod-like architecture (Fig. 4). The correlation to the mineral content of the SBP lessened from 77% within the first millimetre to 45% of the third millimetre (Table 1).

DA

We found an area of isotropic constellation below the posterior and middle parts of the GC within the first layer of VOIs. This behaviour changed into a more anisotropic state with depth accounting for an increase of interconnections. The inferior part as well as areas within the periphery showed higher values expressing a more anisotropic state from the first to the third millimetre. The distribution pattern persisted down to the third layer, while the differences between maximum and minimum reduced gradually (Fig. 4). The correlation coefficient was the lowest for this parameter (0.5 for the first millimetre down to 0.05 for the third millimetre) (Table 1).

Discussion

The cornerstone of the presented data is the concept of functional adaptation of the musculoskeletal system. In detail, it is the fact that bone, as rigid as it is, is a dynamic component within the human body that adapts to its biomechanical impact over time.

The basis and initial foundation of this concept clearly is the work of Julius Wolff, who, in his 1892 published main work, described the functional adaptation and transformation of bone in accordance to the biomechanical demands [34].

As the main tool for the analysis, the method of CT-OAM was used to provide an insight into the long-term biomechanical loading history of every individual sample of the GC. By the visualization of the density distribution, as it is acquired through conventional CT investigations, the mineralization as mirror of the long-term loading history resembles the biomechanical situation within the GC and supports the fact that the SBP as dynamic component transmits forces from the joints' surface down into the TN and optimally adapts to its biomechanical needs. Since in healthy GCs the main overall load is transmitted onto the middle anterior rim and the posterior parts, CT-OAM revealed the densest areas to be situated within these locations accounting for a high mineralization in a mono- and bi-centric pattern [19]. An exceptional position can be seen in people with regularly pitching activities such as baseball players. Here, the percentage of high-density regions within the glenoid cavity is significantly higher than in controls [30].

The above-described results of glenoid mineralization within the healthy population match the findings of Lehtinen et al. as well as Frich et al. Both described the total mineralization in the glenoid as significantly greater superiorly than inferiorly and posteriorly than anteriorly, the ratio being 2:1. The same was noted for trabecular mineralization beneath the SBP. Although the specimen age of their study was quite high, they believe aging does not cause regional mineralization changes in normal healthy shoulders and therefore, the anatomic distribution and differences of the mineral content can be used in the younger population as well [12, 20]. In contrast to this data and as proof of the anatomical adaptation towards the long-term load intake, Schulz et al. investigated the mineral distribution of the glenoid cavity in patients with recurrent anterior glenohumeral dislocation of at least 1 year. In their study, they revealed a significant change of glenoid density maxima positions with an increased anterior and inferior density when compared with normal joints indicating an altered stress distribution on the glenoid toward anterior and inferior in the direction of humeral head translation [29].

Given the anatomical properties of the glenoid, it is to say that in general, it differs in height between male

(38 ± 3 mm) and female (32 ± 1.4 mm) as well as in width (male 28 ± 3 mm; female 24 ± 3 mm) [27]. The articulation surface cannot be seen as a simple axial plane. Within itself, it shows a version from superior-to-inferior and therefore presents a spiralling twist which is shown to be age independent [2]. The glenoid rotation nevertheless, proved to have no significant differences between sexes. On the microanatomic level, the SBP shows a functional adaptation to the long-term biomechanical situation with its mechanical properties adapting to it. Not only is the thickness of the SBP the highest in areas of high mineral content as our study proofs, but also the cartilage thickness shows a maximum of distribution here [36].

The TN below the SBP also revealed structural properties in accordance to the biomechanical situation represented by CT-OAM and, interestingly, we observed the bi-centric and monocentric pattern as well. Although it is not as impressively distinct and obvious as in the SBP, we can confirm that the trabecular architecture has adapted to the biomechanical situation in a way where anatomical-defined structural parameters which describe an accumulation of bone to maximize the support were found to have peak values just beneath areas of high mineralization as it has been shown in literature before on other joints. A similar adaptation of trabecular bone to long-term load has previously been described at the ankle joint, the patellofemoral joint and the knee, to name just a few [14, 26, 35]. The above-described distribution pattern of the glenoid cavity, in correlation to the mineralization, persistent into depth but revealed a dwindling effect.

Altogether, one can say, that the TN, in its way to support the SBP, adapts to its needs using as much material as necessary and as less as possible. Interestingly, the parameters also showed a more homogenous distribution within the depth of third millimetre than just below the SBP. Following Wolff's law, this can be seen as adaptation to the more equally distributed forces within the depth of the bone in comparison to just beneath the articular surface.

The results clearly support the hypothesis that the TN, in its function to support the SBP, adapts to its biomechanical needs according to the long-term load intake of the shoulder joint. The described results are interpreted as an architectural behaviour in dependence to the applied tensile forces and to ideally meet the biomechanical demands.

The described structural findings are in strong consent to the "Mechanobiology hypothesis" of Carter et al. [3, 4]. Here, the adaptation of bone within the living is mainly dependent on two major components. The biological component describes the genetic disposition which mainly influences the development during the growth period and lessens on effect in the adultery. The mechanical component is described to be of main influence once the growth period is finished and afterwards models bone in a way to obtain the strain levels. Single load intake moments which are defined as "loading history" over a certain impact of time are summarized as strain energy density. On a microstructural level, the long-term load intake triggers a fluid flow within the bone's widely spaced lacunae interconnected by canaliculi and produces an oscillatory fluid flow which stimulates a cell response. Streaming potentials, chemo-transport as well as wall shear stresses are seen as the triggers that cause cell deformation and therefore subsequent metabolic activity [17, 33]. This way, the system administers the deficient expression of each structural parameter within the trabecular network. Following the fact that the strain energy density is more and more evenly distributed as it gets transfered through the SBP and the trabecular network administers the changes from a high degree of differentiation just beneath the SBP to a more equal distribution within the deeper areas. In the end, the bone produces a state of homeostasis between structural arrangement and the strain energy density which we tried to illustrate with this study.

After all, the biomechanical situation of a joint as it can be administered via CT-OAM gives direct conclusion about the anatomical configuration of the bone below the joints surface. This knowledge, acquired via conventional CT data, might help in the decision-making process of implant design and implant fixation, since the survival of the glenoid implant is dependent on the biomechanical elements like bone properties and loading location. Preoperative identification of shoulders with eccentric loading of the glenoid and following differences in trabecular arrangement, could explain the postoperative glenoid loosening as it is described in literature [31].

Limitations of the study

The absolute bony mineralization differed at an individual level. Possible explanations are pathologically related changes affecting bone metabolism such as osteoporosis, hormonal disturbances, immobilization, but also physiological differences such as physical activity, weight, gender, and age

In addition, the small quantity and the lack of detailed documentation regarding the former lifestyle does not allow definitive interpretation of the inter-individual measurement results.

Future studies, as they are already planned, will have to address the anatomical subchondral situation in a pathological setting. Also, racial differences as well as anatomic variants have been observed regarding the mineral distribution of other joints which will have to be considered and tested at the shoulder.

Acknowledgements We would like to thank the "Swiss National Science Foundation" for supporting our research with the Grant 316030_133802/1.

Author contributions SH and MM-G designed the study. The acquisition of data was achieved by TAZ and MT. SH and TAZ were in charge of the analysis and interpretation process of drafting and revising the manuscript. All authors finally approved the submitted version.

Compliance with ethical standards

Conflict of interest The authors declare that they have no financial and personal relationships with other people or organizations that could inappropriately influence their work.

References

1. Birkenhäger-Frenkel D, Courpron P, Hüpscher E, Clermonts E, Coutinho M, Schmitz P, Meunier P (1988) Age-related changes in cancellous bone structure. A two-dimensional study in the transiliac and iliac crest biopsy sites. Bone Miner 4:197–216
2. Bouchaib J, Clavert P, Kempf J-F, Kahn J-L (2014) Morphological analysis of the glenoid version in the axial plane according to age. Surg Radiol Anat 36:579–585
3. Carter DR (1984) Mechanical loading histories and cortical bone remodeling. Calcif Tissue Int 36:S19–S24
4. Carter DR, Beaupré GS (2007) Skeletal function and form: mechanobiology of skeletal development, aging, and regeneration. Cambridge University Press, Cambridge
5. Cheal E, Snyder B, Nunamaker D, Hayes W (1987) Trabecular bone remodeling around smooth and porous implants in an equine patellar model. J Biomech 20:1121–1134
6. Cowin SC (2001) Bone mechanics handbook. CRC Press, London
7. Day J, Ding M, Odgaard A, Sumner D, Hvid I, Weinans H (2000) Parallel plate model for trabecular bone exhibits volume fraction-dependent bias. Bone 27:715–720
8. Dempster DW, Compston JE, Drezner MK, Glorieux FH, Kanis JA, Malluche H, Meunier PJ, Ott SM, Recker RR, Parfitt AM (2013) Standardized nomenclature, symbols, and units for bone histomorphometry: a 2012 update of the report of the ASBMR Histomorphometry Nomenclature Committee. J Bone Miner Res 28:2–17
9. Eckstein F, Muller-Gerbl M, Putz R (1992) Distribution of subchondral bone density and cartilage thickness in the human patella. J Anat 180(Pt 3):425–433
10. Engelke K, Karolczak M, Lutz A, Seibert U, Schaller S, Kalender W (1999) Micro-CT. Technology and application for assessing bone structure. Der Radiol 39:203–212
11. Feldkamp LA, Goldstein SA, Parfitt MA, Jesion G, Kleerekoper M (1989) The direct examination of three-dimensional bone architecture in vitro by computed tomography. J Bone Miner Res 4:3–11
12. Frich LH, Odgaard A, Dalstra M (1998) Glenoid bone architecture. J Shoulder Elbow Surg 7:356–361
13. Hildebrand T, Ruegsegger P (1997) Quantification of bone microarchitecture with the structure model index. Comput Methods Programs Biomed 1:15–23
14. Hoechel S, Schulz G, Müller-Gerbl M (2015) Insight into the 3D-trabecular architecture of the human patella. Ann Anat Anat Anz 200:98–104
15. Hoechel S, Wirz D, Muller-Gerbl M (2012) Density and strength distribution in the human subchondral bone plate of the patella. Int Orthop 36:1827–1834
16. Huiskes R, Ruimerman R, Van Lenthe GH, Janssen JD (2000) Effects of mechanical forces on maintenance and adaptation of form in trabecular bone. Nature 405:704–706
17. Jacobs C, Yellowley C, Davis B, Zhou Z, Cimbala J, Donahue H (1998) Differential effect of steady versus oscillating flow on bone cells. J Biomech 31:969–976
18. Kellgren J, Lawrence J (1957) Radiological assessment of osteo-arthrosis. Ann Rheum Dis 16:494
19. Kraljević M, Zumstein V, Hügli R, Müller-Gerbl M (2013) A comparison of subchondral bone mineralization between the glenoid cavity and the humeral head on 57 cadaverous shoulder joints. Surg Radiol Anat 35:295–300
20. Lehtinen JT, Tingart MJ, Apreleva M, Warner JJ (2004) Total, trabecular, and cortical bone mineral density in different regions of the glenoid. J Shoulder Elbow Surg 13:344–348
21. Lim D, Seliktar R, Wee J-Y, Tom J, Nunes L (2006) The effect of the loading condition corresponding to functional shoulder activities on trabecular architecture of glenoid. J Biomech Eng 128:250–258
22. Muller-Gerbl M (1998) The subchondral bone plate. Adv Anat Embryol Cell Biol 141:III–XI (1–134)
23. Muller-Gerbl M, Putz R, Hodapp N, Schulte E, Wimmer B (1989) Computed tomography-osteoabsorptiometry for assessing the density distribution of subchondral bone as a measure of long-term mechanical adaptation in individual joints. Skelet Radiol 18:507–512
24. Muller-Gerbl M, Putz R, Hodapp N, Schulte E, Wimmer B (1990) Demonstration of subchondral density pattern using CT-osteoabsorptiometry (CT-OAM) for the assessment of individual joint stress in live patients. Z Orthop Ihre Grenzgeb 128:128–133. https://doi.org/10.1055/s-2008-1039487
25. Muller-Gerbl M, Weisser S, Linsenmeier U (2008) The distribution of mineral density in the cervical vertebral endplates. Eur Spine J 17:432–438. https://doi.org/10.1007/s00586-008-0601-5
26. Nowakowski AM, Deyhle H, Zander S, Leumann A, Müller-Gerbl M (2013) Micro CT analysis of the subarticular bone structure in the area of the talar trochlea. Surg Radiol Anat 35:283–293
27. Owaydhah WH, Alobaidy MA, Alraddadi AS, Soames RW (2017) Three-dimensional analysis of the proximal humeral and glenoid geometry using MicroScribe 3D digitizer. Surg Radiol Anat 39:767–772
28. Parfitt AM, Drezner MK, Glorieux FH, Kanis JA, Malluche H, Meunier PJ, Ott SM, Recker RR (1987) Bone histomorphometry: standardization of nomenclature, symbols, and units: report of the ASBMR Histomorphometry Nomenclature Committee. J Bone Miner Res 2:595–610
29. Schulz CU, Anetzberger H, Pfahler M, Refior HJ, Müller-Gerbl M (2004) Anterior shoulder instability modifies glenoid subchondral bone density. Clin Orthop 423:259–263
30. Shimizu T, Iwasaki N, Nishida K, Minami A, Funakoshi T (2012) Glenoid stress distribution in baseball players using computed tomography osteoabsorptiometry: a pilot study. Clin Orthop 470:1534–1539
31. Skirving AP (1999) Total shoulder arthroplasty—current problems and possible solutions. J Orthop Sci 4:42–53
32. Soslowsky LJ, Flatow EL, Bigliani LU, Mow VC (1992) Articular geometry of the glenohumeral joint. Clin Orthop 285:181–190
33. Wang L, Ciani C, Doty SB, Fritton SP (2004) Delineating bone's interstitial fluid pathway in vivo. Bone 34:499–509
34. Wolff J (1986) The law of bone remodelling. Springer, Berlin
35. Zumstein V, Kraljević M, Conzen A, Hoechel S, Müller-Gerbl M (2014) Thickness distribution of the glenohumeral joint cartilage: a quantitative study using computed tomography. Surg Radiol Anat 36:327–331
36. Zumstein V, Kraljević M, Hoechel S, Conzen A, Nowakowski AM, Müller-Gerbl M (2014) The glenohumeral joint—a mismatching system? A morphological analysis of the cartilaginous and osseous curvature of the humeral head and the glenoid cavity. J Orthop Res 9:34